refraction than air. A schlieren photograph of the wake flow including nitrous oxide streamlines adjacent to the base region is shown in Fig. 2b. The streamlines appear clear upstream of the plug base, but become fainter after the expansion about the separation corner and along the mixing region. Further, these nitrous oxide streamlines become even fainter as the recompression oblique shock is approached, and are very difficult to see adjacent to the trailing wake. Furthermore, no significant density gradient perpendicular to the nozzle axis is indicated in the neck of the wake. The use of nitrous oxide or other suitable gases for streamline and/or streakline visualization appears to be very promising.

For steady flow, the smokeline is a streamline and can be used in conjunction with the model geometry and shock waves to determine Mach numbers in the flowfield. A simultaneous smokeline and opaque-stop schlieren photograph of the wake is presented in Fig. 3a. By measuring the local deflection and wave angles of the smoke streamlines passing through the recompression shock wave, the Mach numbers immediately ahead of and behind the recompression shock were determined and are shown in Fig. 3a. Dirt deposited on the glass sidewalls from a previous run is also visible in Fig. 3a. A simultaneous smokeline and opaque-stop schlieren photograph of the wake flow using the laser light source and "clean" glass sidewalls is presented in Fig. 3b.

Discussion of Visual and Probe Results from the Large E-D Nozzle PSST

A simultaneous smokeline and opaque-stop schlieren photograph of the planar expansion-deflection nozzle flowfield at its design operating conditions is presented in Fig. 4a The two smokelines are clearly visible in the top half of the photograph. Dirt on the glass sidewalls is also visible just upstream of the recompression shock waves. A comparison of the Mach numbers obtained from the streamline shock wave pattern of Fig. 4a and another photograph, and from total and static pressure measurements is shown in Fig. 4b. The correlation of Fig. 4b is for the Mach number immediately downstream of the recompression shock vs the distance measured along the recompression shock from the nozzle centerline. The agreement between the visual and pressure data is quite good.

Conclusions

Excellent direct photographs of the smoke streamlines were obtained. A composite streamline, shock and expansion wave patterns, was obtained by using nitrous oxide in place of smoke with an ordinary schlieren system and by using smoke with the opaque-stop schlieren system. From the simultaneous streamline-shock and expansion wave pattern, the Mach numbers adjacent to, but outside of, the viscous near wake and far wake were determined without introducing probes into the stream. For the E-D nozzle flow, a correlation of the visual and pressure data for the Mach number immediately downstream of the recompression shock vs distance along the shock from the nozzle centerline was quite good.

References

[1] Mach, L., "Uber die Sichtbarmachung von Luftstromlinien," *Zeitschrift fur Luftschiffahrt and Physik der Atmosphare*, Vol. 15, No. 6, 1896, pp. 129–139, plates I–III.

[2] Goddard, V. P., McLaughlin, J. A., and Brown, F. N. M., "Visual Supersonic Flow Patterns by Means of Smoke Lines," *Journal of the Aerospace Sciences*, Vol. 26, No. 11, Nov. 1959, pp. 761–762.

[3] Mueller, T. J., Hall, C. R., Jr., and Sule, W. P., "Experiments on the Two-Dimensional Expansion-Deflection Nozzle," AEDC-TR-67-279, Dec. 1967, Arnold Engineering Development Center, Air Force Systems Command, USAF.

Current Ratios in Coaxial Plasma Accelerators

R. P. Henry*
University of Ottawa, Ottawa, Canada

AND

D. S. Scott†
University of Toronto, Toronto, Canada

SINCE the generation of very large Hall currents may be important in certain types of coaxial plasma accelerators, plasma states yielding the most favorable conditions require investigation. Practical physical limitations usually restrict the current that may be carried by electrodes; however the Hall current, which is electrodeless and circulates within the body of the plasma, does not contribute as severely to electrode surface heating and resulting ablation problems.

Conditions yielding maximum Hall-to-applied currents may be calculated using a suitable generalized Ohm's law. In this Note, results based on the simple Cowling's law[1] are compared with a second approximation given by Demetriades and Argyropoulos.[2] This latter expression, developed by solving the Boltzmann equations according to Grad's "thirteen-moment" method, includes effects of electron-electron interactions and produces a more accurate determination of the inter-particle friction factors. Improved accuracy in the expression for scalar conductivity results.

When pressure and temperature gradients in the three-species plasma are neglected, both Ohm's laws assume the same form,

$$\mathbf{E}' = (1/\sigma)\mathbf{J} + \chi(\mathbf{J} \times \mathbf{B}) - \psi(\mathbf{J} \times \mathbf{B}) \times \mathbf{B} \tag{1}$$

however, expressions for σ, χ, and ψ, the scalar conductivity, Hall coefficient, and ion slip coefficient differ. Now the factors in the square brackets of the following equations are no longer unity;

$$\frac{1}{\sigma} = \frac{m_e}{n_e e^2}\frac{1}{\tau_0}\left[1 - \frac{5}{2}\upsilon_0{}^2\tau_0\tau_e{}^*\right] \tag{2}$$

$$\chi = \frac{1}{n_e e}\left[1 + \frac{5}{2}\upsilon_0{}^2\left(\frac{\tau_e{}^{*2}}{1 + \omega_e{}^2\tau_e{}^{*2}}\right)\right] \tag{3}$$

$$\psi = \frac{2f^2}{n_e m_a}\tau_{ia}\left[1 + \frac{5}{4}\frac{m_a\tau_e{}^*}{f^2 m_e\tau_{ia}}\upsilon_0{}^2\left(\frac{\tau_e{}^{*2}}{1 + \omega_e{}^2\tau_e{}^{*2}}\right)\right] \tag{4}$$

Collisions parameters υ_0 and $\tau_e{}^*$ are as defined in Ref. 2.

When use is made of Eq. (1), the expression for the ratio of Hall-to-electrode current is the same, except for a factor based on geometry, in the two common Hall current plasma accelerator configurations.[3] For a coaxial electrode geometry with axially applied magnetic field,

$$J_\theta/J_r = \chi\sigma B/(1 + \psi\sigma B^2) \tag{5}$$

Introducing $\beta = \chi_0\sigma_0 B$ and $x = \chi_0{}^2\sigma_0/\psi_0$, where the subscript 0 refers to the Ohm's law coefficients in Cowling's expression, and

$$k_1 = \tfrac{5}{2}\upsilon_0{}^2\tau_0\tau_e{}^*, \quad k_2 = \tfrac{5}{2}\upsilon_0{}^2\tau_e{}^{*2}, \quad k_3 = \tfrac{5}{2}\upsilon_0{}^2\tau_e{}^{*3}/\tau_0 \tag{6}$$

Presented as Paper 69-280 at the AIAA 7th Electric Propulsion Conference, Williamsburg, Va., March 3–5, 1969; submitted March 12, 1969; revision received July 25, 1969.

* Assistant Professor, Mechanical Engineering Department. Member AIAA.

† Associate Professor, Mechanical Engineering Department. Member AIAA.

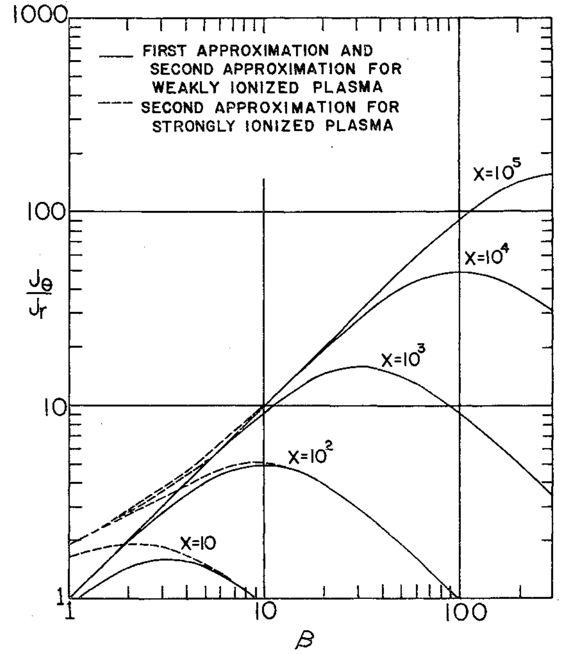

Fig. 1 Typical curves of Hall-to-electrode current ratios vs β.

then

$$\frac{J_\theta}{J_r} = \frac{\left[\frac{1}{1-k_1}\left(1+\frac{k_2}{1+\{(k_2/k_1)\beta\}^2}\right)\right]\beta}{\left\{1+\left[\frac{1}{1-k_1}\left(1+\frac{xk_3}{1+\{(k_2/k_1)\beta\}^2}\right)\right]\frac{\beta^2}{x}\right\}} \qquad (7)$$

This expression differs from that obtained using Cowling's law by the terms in the square brackets, which previously were unity.

Equation (7) does not lend itself readily to the determination of an analytical expression for its maximum, with respect to B, as is possible with the simpler first-approximation result. Calculations for several collision models are shown in Fig. 1. Here it may be seen that over a wide range of parameters there is essentially no difference between the

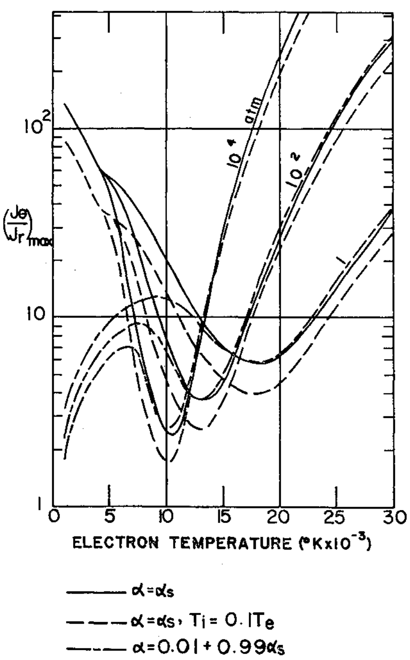

Fig. 2 Maximum Hall-to-electrode current ratios for three plasma models.

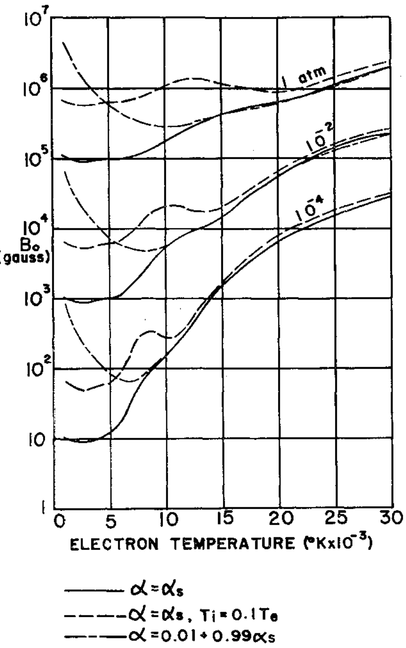

Fig. 3 Magnetic field requirements corresponding to maximum Hall-to-electrode current curves of Fig. 2.

two approximations even for a strongly ionized plasma. The magnetic field corresponding to the maximum of each curve is also the same in both approximations. The weak dependence of J_θ/J_r upon the order of the approximation is interesting in view of the fact that χ and ψ are strongly dependent upon the order.

To determine the influence of various phenomena on accelerator performance, the following cases are considered:

1) Equilibrium, such that ionization fraction α_s may be calculated using the Saha equation.

2) To simulate preionization or "seeding" effects a minimum of 1% ionization is imposed on the model. Ionization fraction is calculated using $\alpha = 0.01 + 0.99\ \alpha_s$.

3) The effect of nonequilibrium electron temperature T_e is considered by introducing a model in which T_e is ten times the heavy species temperature. Ionization fraction is calculated using the Saha equation at T_e.

Collision data from a number of recent sources, suitably thermally averaged, have been used to evaluate collision parameters. Graphical results of $(J_\theta/J_r)_{max}$ and the corresponding magnetic fields B_0 are presented in Figs. 2 and 3. In thermodynamic equilibrium, it is apparent that the maximum Hall current ratios may be approximately divided into three regions, based on electron temperature and characterized as follows:

1) A region of low ionization and temperature in which electron-neutral collisions dominate. This region is characterized by high values of maximum Hall-to-electrode current ratios and relatively low magnetic field requirements. Conductivity, however, is so low as to make this region impractical for accelerator use.

2) An intermediate ionization and temperature region in which conductivity is appreciable, electron-ion collisions dominate, but maximum Hall-to-electrode current ratios fall to quite low values.

3) A region of high temperature and ionization level in which maximum Hall-to-electrode current ratios rise to large values, but magnetic field requirements increase substantially and extreme temperatures present physical problems.

A comparison of the conditions and models chosen for study also suggests other important conclusions. Magnetic field requirements to achieve maximum current ratios increase approximately in proportion to increased plasma pressure. Plasma preionization or "seeding" is ineffectual in increasing current ratios and in fact decreases them in region 1 where these greater conductivity techniques are most useful. Comparison on the basis of the same electron temperature indicates that a nonequilibrium plasma will have slightly lower maximum current ratios than one in equilibrium. The former situation, however, may permit much higher temperature operation, far to the right in region 3 where maximum current ratios increase sharply. Similar calculations with helium indicate the same trends except that maximum current ratios are nearly one order of magnitude lower in region 1 whereas regions 2 and 3 begin at higher electron temperatures.

A one-dimensional coaxial device has been built to qualitatively check some of these theoretical predictions. Some preliminary experimental results described in Ref. 4 tend to substantiate them, although current ratios obtained up to this time have not been as large as expected.

References

[1] Cowling, T. C., *Magnetohydrodynamics*, Interscience, New York, 1957.

[2] Demetriades, S. T. and Argyropoulos, G. S., "Ohm's Law in Multicomponent Nonisothermal Plasmas with Temperature and Pressure Gradients," *The Physics of Fluids*, Vol. 9, 1966, pp. 2136–2149.

[3] Henry, R. P., "Lorentz Force Maximization in Continuous Flow Hall Current Plasma Accelerators," *AIAA Journal*, Vol. 4, No. 1, Jan. 1966, pp. 165–166.

[4] Henry, R. P. and Scott, D. S., "Ion-Slip Limitations on Currents in Hall-Effect Plasma Accelerators," UTME-TP 6805, June 1968, Department of Mechanical Engineering, University of Toronto, Canada.

A Multiple Time Scaling Analysis of Re-Entry Roll Dynamics

Ali Hasan Nayfeh*
Aerotherm Corporation, Mountain View, Calif.

1. Introduction

THE rigid-body motion of a body entering the atmosphere depends upon many factors, such as the initial conditions, the mass and mass distribution, the external geometry, and the heat shield material. Since, in practice, vehicles have varying degrees of asymmetries, there is a coupling of the pitch and yaw degrees of freedom with the roll degree of freedom. The resultant heating and ablation will be asymmetric and new asymmetries will be induced.

Most theories for rolling symmetrical missiles have made use of the basic ballistic analysis of Fowler et al.,[3] Nicolaides,[9] and Charters[1] obtained theories for rolling missiles having slight configurational asymmetries using nonrolling coordinate systems. Nelson[8] obtained a theory for slightly asymmetrical missiles using a body-fixed coordinate system. However, all of these theories, like that of Fowler, are linear and assume constant roll rate and freestream conditions. Coakley,[2] on the other hand, obtained a solution for the time variations of the angle of attack of rolling symmetrical missiles using the WKBJ method.[4] In Ref. 2, the roll rate is decoupled from the other degrees of freedom but the time variation of the freestream conditions is accounted for.

In this Note, approximate solutions are obtained for the roll rate and angle of attack for missiles with slight center of gravity and aerodynamic trim asymmetries using the method of multiple time scales.[5,6] The time variation of the freestream conditions as well as the coupling of the roll rate with the other degrees of freedom are taken into account. The analysis is based upon the observation that there are at least two time scales: a slow time characterizing the variation of the dynamic pressure and a fast time characterizing the angle-of-attack oscillations.

It is assumed that gravity forces are negligible, and the aerodynamic forces and moments are linear. Velocities, atmospheric density, and time are made dimensionless using the entry velocity u_e, sea-level density ρ_s, and characteristic time $T = [2I/\rho_s u_e^2 Ad]^{1/2}$, where I is the transverse moment of inertia and d and A are the body diameter and cross-sectional area, respectively.

A right-handed orthogonal body-fixed coordinate system is introduced such that the x axis is the longitudinal axis, the y axis is the horizontal transverse axis, and the z axis is orthogonal to the x and y axes. The velocity components along these axes are denoted by u, v, and w, and the angular velocities about these axes are denoted by p, q, and r, respectively. The six-degree-of-freedom equations of motion can be transformed into[7]

$$\dot{u} + qw - rv = -\epsilon\rho V^2 \tag{1}$$

$$\dot{p} = \rho V^2[\epsilon C_{l0} + C_{N\alpha}\alpha c/d + \epsilon\nu C_{lp}p/V]/(1-\gamma) \tag{2}$$

$$\ddot{\delta} + [ip(1+\gamma) + \dot{u}/u + \epsilon Q - \epsilon D]\dot{\delta} + [i\dot{p} + \gamma(p_c^2 - p^2) + ip(\gamma\dot{u}/u - \epsilon D - \epsilon M + \epsilon\gamma Q/u)]\delta - \gamma\tilde{\delta}_t + 0(\epsilon^2\delta) = 0 \tag{3}$$

where the complex angle of attack $\delta = \beta + i\alpha$, $p_c^2 = -\rho V^2 C_{m\alpha}/\gamma$, $\gamma = 1 - I_x/I$, $Q = \rho V^2 C_{N\alpha}/C_D$, $D = \rho V\nu(C_{m\dot{\alpha}} + C_{mq})$, $M = \rho V\nu C_{mp\alpha}$, $\nu = md^2/2IC_D$, $\epsilon = [\rho_s I/2Ad]^{1/2}/B$, and $B = m/C_D A$. Here, C_D is the drag coefficient, C_{lp} is the roll damping coefficient, C_{l0} is the pure roll torque coefficient, $C_{m\alpha}$ and $C_{mp\alpha}$ are the pitching and Magnus moment coefficients, C_{mq} and $C_{m\dot{\alpha}}$ are the pitch or yaw damping derivatives, $C_{N\alpha}$ is the normal force derivative, I_x is the axial moment of inertia, m is the vehicle mass, and V is the absolute velocity.

2. Analysis

Actual flight test data and six-degree-of-freedom numerical calculations show that there are at least two time scales: a slow time characterizing the variation of velocity and a fast time characterizing the angle-of-attack oscillations. This suggests the applicability of the method of multiple scales[5,6] to determine an asymptotic solution for Eqs. (1–3) for small ϵ.

Introduce a slow time $\tau = \epsilon t$ and a fast time $\eta = g(\tau)/\epsilon$ where $g(\tau)$ is an unknown function that will be determined in the course of analysis. Assume that $\tilde{\delta}_t = \epsilon\delta_t$, and u, p, and δ possess the following expansions:

$$u(t) = u_0(\tau,\eta) + \epsilon u_1(\tau,\eta) + \ldots \tag{4}$$

$$p(t) = p_0(\tau,\eta) + \epsilon p_1(\tau,\eta) + \ldots \tag{5}$$

$$\delta(t) = \epsilon\delta_1(\tau,\eta) + \epsilon^2\delta_2(\tau,\eta) + \ldots \tag{6}$$

Substitute these expansions into Eqs. (1–3) and equate coefficients of equal powers of ϵ. The solutions of the resulting equations contain arbitrary functions of τ. These functions as well as $g(\tau)$ will be determined by requiring that Eqs. (4–6) be uniformly valid expansions; i.e., the second terms are small corrections to the first terms. Thus, it is required that u_1/u_0, p_1/p_0, and $\delta_2/\delta_1 < \infty$ for all η and τ.

The zeroth-order equations lead to

$$u_0 = u_0(\tau) \text{ and } p_0 = p_0(\tau) \tag{7}$$

Therefore, Q, M, D, p_c, and C_{l0} are functions of the slow time

Received December 10, 1968; revision received June 9, 1969.

* Manager, Mathematical Physics Department. Member AIAA.